Propagation properties of quasi-periodic VLF emissions observed by the DEMETER spacecraft

Mykhaylo Hayosh, František Němec, Ondřej Santolík, Michel Parrot

AGU PUBLICATIONS

Geophysical Research Letters

RESEARCH LETTER
10.1002/2015GL067373

Key Points:
- ELF QP emissions can propagate unducted down to the low Earth orbit
- QP waves predominantly propagate radially toward Earth at latitudes up to ±65 degrees
- The Poynting vector is inclined from the equator at magnetic latitudes within ±20 degrees

Correspondence to:
M. Hayosh,
hayosh@ufa.cas.cz

Citation:
Hayosh, M., F. Němec, O. Santolík, and M. Parrot (2016), Propagation properties of quasiperiodic VLF emissions observed by the DEMETER spacecraft, *Geophys. Res. Lett., 43*, doi:10.1002/2015GL067373.

Received 11 DEC 2015
Accepted 13 JAN 2016
Accepted article online 16 JAN 2016

Propagation properties of quasiperiodic VLF emissions observed by the DEMETER spacecraft

Mykhaylo Hayosh[1], František Němec[2], Ondřej Santolík[1,2], and Michel Parrot[3]

[1]Department of Space Physics, Institute of Atmospheric Physics, CAS, Prague, Czech Republic, Prague, UK, [2]Faculty of Mathematics and Physics, Charles University in Prague, Prague, Czech Republic, [3]LPC2E/CNRS, Orléans, France

Abstract Quasiperiodic (QP) emissions are electromagnetic waves in the frequency range of about 0.5–4 kHz observed in the inner magnetosphere that exhibit a periodic time modulation of the wave intensity, with modulation periods from a few seconds up to 10 min. We present results of a detailed wave analysis of nearly 200 events measured by the low-altitude Detection of Electro-Magnetic Emissions Transmitted from Earthquake Regions (DEMETER) spacecraft. Upper frequency range of studied emissions was limited to 1 kHz due to the sampling rate of the analyzed data. It is found that QP emissions propagate nearly field aligned at larger geomagnetic latitudes; they become more oblique at midlatitudes and eventually perpendicular to the ambient magnetic field at the geomagnetic equator and thus perpendicular to the Earth's surface, allowing their downward propagation through the ionosphere. The observed propagation pattern is consistent with the source of emissions located in the equatorial region at larger radial distances.

1. Introduction

Quasiperiodic (QP) emissions are whistler-mode electromagnetic waves observed in the inner magnetosphere, mostly on its dayside. The amplitude of these waves has a periodic time modulation. We have analyzed QP events with modulation periods more than 10 s. Such QP emissions can be, according to *Sato et al.* [1974], divided into two classes. Emissions of the first class (QP1) are associated with ULF magnetic field pulsations and the intensity modulation is a result of the whistler-mode wave growth in the generation region being periodically modulated by the pulsations [*Kitamura et al.*, 1968; *Sato and Kokubun*, 1980; *Sato and Fukunishi,* 1981; *Sazhin,* 1987]. Emissions of the second class (QP2) are observed in the absence of ULF magnetic field pulsations. Generation of these emissions was explained in the frame of relaxation oscillations of the cyclotron instability [*Bespalov and Trakhtengerts*, 1976; *Davidson*, 1979] or as a result of the autooscillation regime of wave generation [*Demekhov and Trakhtengerts*, 1994; *Pasmanik et al.*, 2004]. QP events might be associated with precipitation of high-energy electrons [*Kitamura et al.*, 1969; *Sato et al.*, 1974; *Manninen et al.*, 2012, 2014]. Simultaneous observations of QP emissions and precipitating energetic electrons by the Detection of Electro-Magnetic Emissions Transmitted from Earthquake Regions (DEMETER) spacecraft were reported by *Hayosh et al.* [2013], confirming a suitability of such generation mechanism.

Temporal and spatial properties of QP emissions were experimentally analyzed in case studies and statistical surveys, using both ground-based and satellite data [*Ho,* 1973; *Kimura,* 1974; *Tixier and Cornilleau-Wehrlin,* 1986; *Morrison et al.*, 1994; *Hayosh et al.*, 2013; *Němec et al.*, 2013a]. The reported modulation period varies from several seconds to several minutes. The emissions may be observed for up to several hours, at L shells from about 2 to 8 and in a frequency range of 500 Hz–4 kHz [*Helliwell,* 1965; *Carson et al.*, 1965; *Morrison et al.*, 1994; *Engebretson et al.*, 2004; *Manninen et al.*, 2013]. However, the wave propagation parameters of QP emissions were estimated only for a few events [*Němec et al.*, 2013a, 2013b].

In the present study, we statistically analyze the wave propagation parameters based on the DEMETER spacecraft data, and we attempt to explain the observed dependencies. The used data set and the analyzed characteristics of QP emissions are described in section 2. The obtained results are presented in section 3. Finally, section 4 contains a brief discussion and summary of the main results.

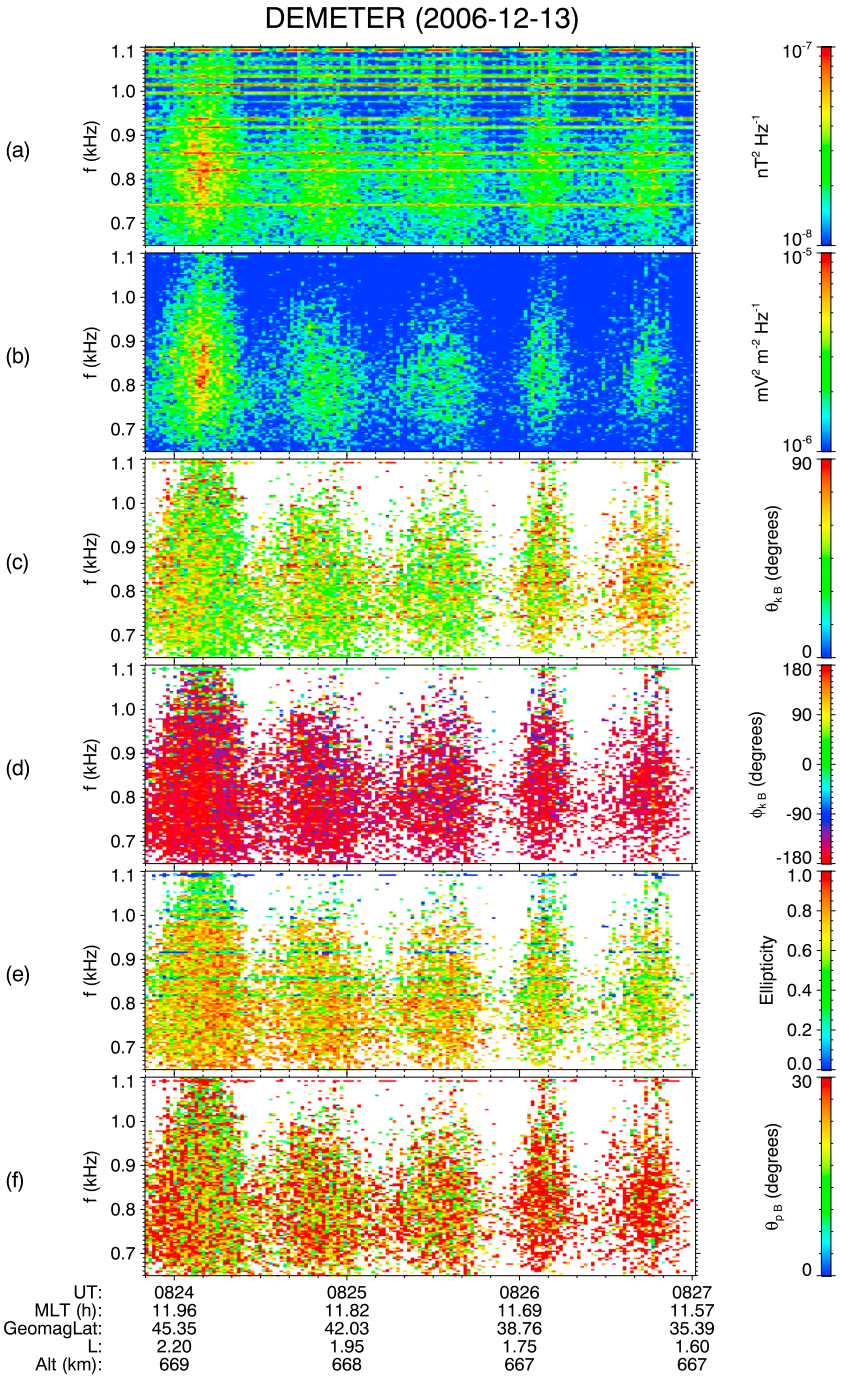

Figure 1. Frequency-time spectrogram of a QP event measured on 13 December 2006. (a, b) Power spectral density of magnetic and electric field fluctuations, respectively; (c) Frequency-time plot of the polar angle θ_{kB} between the wave vector direction and $\mathbf{B_0}$; (d) Frequency-time plot of the angle φ_{kB}, corresponding to the azimuth of the wave vector; (e) Frequency-time plot of the ellipticity of magnetic field fluctuations; (f) Frequency-time plot of the polar angle θ_{pB} between the Poynting vector direction and $\mathbf{B_0}$.

2. Data

The French microsatellite DEMETER was launched in June 2004, and it was operated until December 2010. The spacecraft had a nearly Sun-synchronous circular orbit (LT ≈ 10.30 and ≈ 22.30) at an altitude of about 700 km. It performed 14 orbits per day, providing measurements at geomagnetic latitudes from −65° to 65°.

We have used the list of 2264 QP events identified in the DEMETER data collected from 2004 to 2010 [*Hayosh et al*., 2014]. A detailed analysis of the wave propagation and polarization characteristics requires simultaneous measurements of all six components of the electromagnetic field [*Santolík et al*., 2006a]. Such data were measured by DEMETER in the Burst mode. The frequencies lower than 1 kHz were selected by a low-pass filter and recorded with the sampling frequency of 2.5 kHz [*Parrot et al*., 2006; *Berthelier et al*., 2006]. However, the Burst mode was turned on irregularly, mostly above regions of a special interest. This limits our analysis to only 196 QP events. Note that the data for all frequencies were combined in a single data set. Given the applied intensity threshold, the frequency ranges of the individual events and the time durations of the burst mode intervals, the final data set contains in total over 4 million data points.

The wave analysis is done in a coordinate system linked to the local magnetic field $\mathbf{B_0}$. The $\boldsymbol{z}$ axis is oriented along $\mathbf{B_0}$; the $\boldsymbol{x}$ axis is in the local meridian, and it points toward larger L values, and the $\boldsymbol{y}$ axis completes the orthogonal system. The wave vector direction and the ellipticity of the magnetic field fluctuations were determined using singular value decomposition of the spectral matrix [*Santolík et al*., 2003]. The direction of the wave vector $\boldsymbol{k}$ is characterized in spherical coordinates by the polar angle θ_{kB} and the azimuthal angle φ_{kB}. The value of θ_{kB} varies between 0° and 180° with respect to $\mathbf{B_0}$ and the value of φ_{kB} varies between 180° and −180°, with the value of 0° corresponding to the direction of increasing L. The absolute value of ellipticity is defined as the ratio of the minor to major axes of the polarization ellipse, and its sign corresponds to the polarization sense [*Santolík et al*., 2002]. For left-handed circularly polarized waves the ellipticity is thus equal to −1; a value of 1 corresponds to the right-handed circular polarization. The ellipticity of linearly polarized waves is equal to 0. The Poynting vector is calculated from electromagnetic cross spectra using method of *Santolík et al.* [2001]. Analogically to the wave vector, its direction is defined by the polar angle θ_{pB} and the azimuthal angle φ_{pB}. Values of $\theta_{pB} < 90°$ correspond to the parallel propagation with respect to $\mathbf{B_0}$, while values of $\theta_{pB} > 90°$ correspond to the antiparallel propagation.

3. Results

Each of the selected 196 QP events was analyzed in detail. First, frequency-time spectrograms of the power spectral densities of the wave electric and magnetic fields were plotted for each event. Based on these spectrograms, the time intervals corresponding to the QP emissions and their frequency ranges were manually determined. The wave analysis is limited to the frequencies lower than 1 kHz due to the limitations of the Burst mode multicomponent data. Second, electric field power-spectral density thresholds were selected separately for each event in such a way that background was below these thresholds, while QP emissions were more intense than these thresholds. The thresholds varied between 10^{-7} and 10^{-4} $mV^2\,m^{-2}\,Hz^{-1}$ throughout our data set. This allowed us to select only frequency-time intervals corresponding to the QP elements. The appropriate spectral matrices were calculated using a discrete Fourier transformation computed over time interval of 768 six-dimensional samples, with 50% overlapping, and averaging over four neighboring time intervals. These spectral matrices have been used as input data in the procedures for the calculation of the wave propagation parameters. Finally, the propagation properties calculated for all 196 events were combined in one data set for the purpose of this study. The geomagnetic latitude of the measurements is the main controlling factor of the observed propagation properties. We thus classify the observations according to their geomagnetic latitude in 2° large bins, and we evaluate the probability density function of each analyzed propagation parameter in each latitudinal bin. This approach allows us to effectively combine all 196 events in one plot per each propagation parameter.

An example of QP emissions measured by DEMETER on 13 December 2006, along with the results of the wave analysis, is presented in Figure 1. The calculated values of the wave parameters are color coded as a function of frequency and time. The times and locations of the measurements are given on the abscissa axis. The total observed duration of the event was about 12 min, but the Burst mode required for the detailed wave analysis was turned on only between 0823.50 and 0827.00 UT (the time interval shown in the figure). The spacecraft was located in the Northern Hemisphere and moving southward. The geomagnetic latitude decreases from ~45° to ~35°, corresponding to L shell variation from about 2.2 to 1.6.

The frequency-time spectrograms of power spectral density of magnetic and electric field fluctuations are shown in Figures 1a and 1b, respectively. The quasiperiodic modulation period of the event is about 32 s. Figures 1c and 1d represent the frequency-time plots of θ_{kB} and φ_{kB}, respectively. The wave vector direction

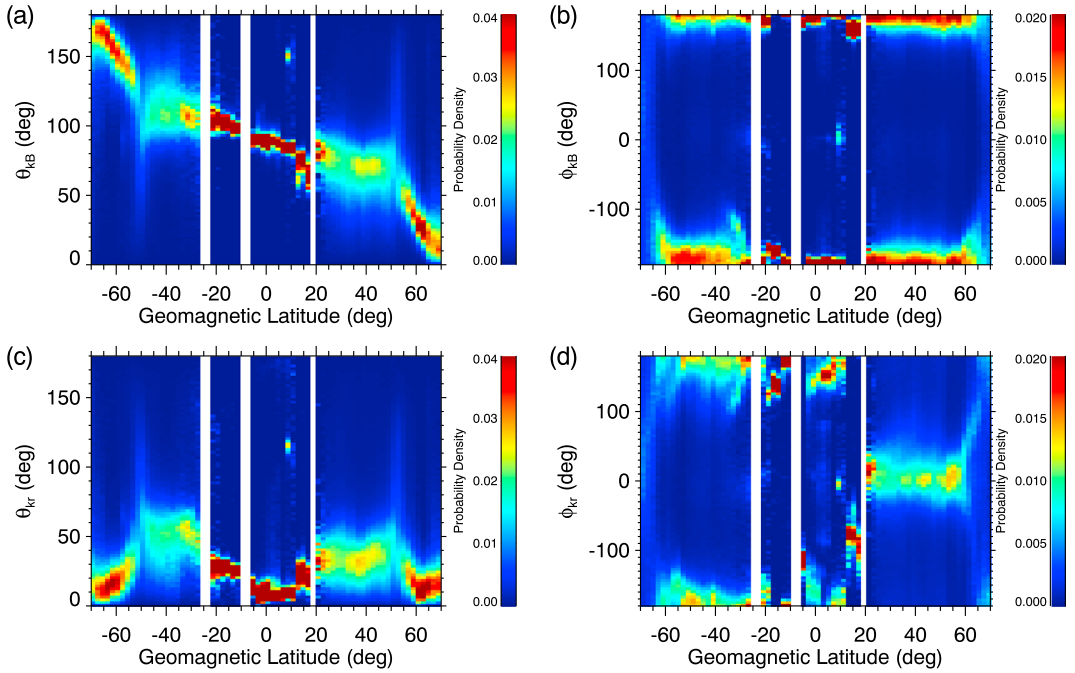

Figure 2. (a) Distribution of the polar angle θ_{kB} between the wave vector direction and $\mathbf{B_0}$ as a function of the geomagnetic latitude. Values lower than 90° correspond to the orientation along the ambient magnetic field, while the values larger than 90° correspond to the orientation opposite to the ambient magnetic field. (b) Distribution of the azimuthal angle φ_{kB} of the wave vector direction as a function of the geomagnetic latitude. The values of $\varphi_{kB} = \pm 180°$ correspond to the direction of decreasing *L* values. (c) Distribution of the polar angle θ_{kr} between the wave vector direction and the direction toward the Earth's center as a function of the geomagnetic latitude. (d) Distribution of the azimuthal angle φ_{kr} of the wave vector with respect to the vertical direction as a function of the geomagnetic latitude. The value of $\varphi_{kr} = 0°$ corresponds to the southward direction of the wave vector and the value of $\varphi_{kr} = 90°$ corresponds to its westward direction. Plots are based on 196 events measured during 2004–2010. Vertical white stripes correspond to data gaps caused by limited data coverage of the burst mode measurements.

is oblique to $\mathbf{B_0}$ ($30° \leq \theta_{kB} \leq 70°$) during the whole time interval. The values of φ_{kB} are close to ±180°, corresponding to the orientation toward lower L shells. The ellipticity of the polarization of magnetic field fluctuations is larger than 0.5, corresponding to the right-handed almost circularly polarized wave (Figure 1e). The angle θ_{pB} varies between about 20° and 50° (Figure 1f). Taking into account the orientations of both wave and Poynting vectors and the Earth magnetic field, we can summarize that the waves propagate obliquely to the ambient magnetic field, toward the Earth (deviating toward lower L shells) and becoming slightly more oblique at lower geomagnetic latitudes.

The statistical distribution of the angles θ_{kB} and φ_{kB} as a function of the geomagnetic latitude is color coded in Figures 2a and 2b, respectively. The probability density function was estimated in such a way that its integral over the entire range of the angle values in any given latitudinal bin is equal to 1. White areas at some latitudes are due to data gaps caused by limited data coverage of the Burst mode measurements. It can be seen in Figure 2b that the azimuthal angles of the wave vector direction are mostly close to ±180°; i.e., the wave vectors are generally oriented toward lower L values and toward the Earth. The distribution of wave normal angles plotted in Figure 2 is symmetric about the geomagnetic equator, as one would expect.

The wave vectors of QP emissions observed at larger geomagnetic latitudes are found to be nearly field-aligned and oriented again toward the Earth. Namely, $\theta_{kB} > \sim 150°$ at the latitudes $< \sim -60°$, and $\theta_{kB} < \sim 30°$ at the latitudes $> \sim 60°$ (Figure 2a). The wave vectors at lower geomagnetic latitudes become gradually more oblique with respect to local field line. The wave normal angle increases abruptly at the geomagnetic latitudes of about ±50°, and the wave vectors are nearly perpendicular to the ambient magnetic field at lower geomagnetic latitudes. It would appear that at the geomagnetic equator the waves propagate principally perpendicular to the ambient magnetic field. Note, however, that the number of data in the analysis at geomagnetic latitudes lower than about 20° is extremely limited.

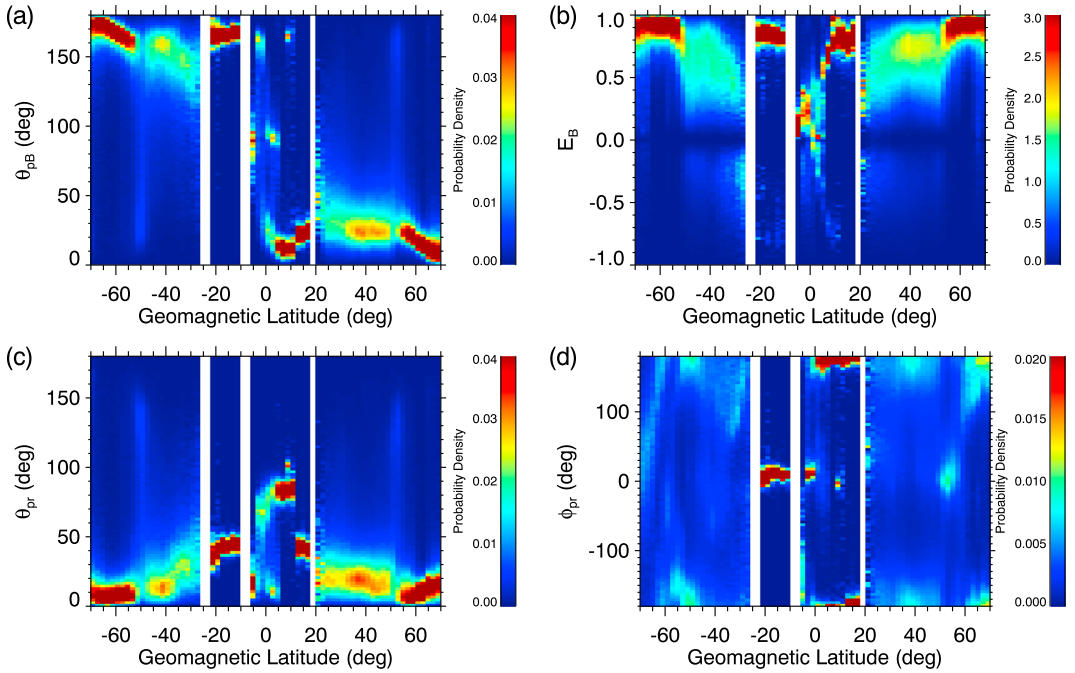

Figure 3. (a) Distribution of the polar angle θ_{pB} between the Poynting vector and the ambient magnetic field as function of the geomagnetic latitude. Values lower than 90° correspond to the propagation along the ambient magnetic field, while the values larger than 90° correspond to the propagation opposite to the ambient magnetic field. (b) Distribution of the ellipticity of magnetic field fluctuations as a function of the geomagnetic latitude. Positive values correspond to the right-handed polarized waves. The absolute values close to 1 correspond to nearly circularly polarized waves. (c) Distribution of the polar angle θ_{pr} between the Poynting vector direction and the direction toward the Earth's center as a function of the geomagnetic latitude. (d) Distribution of the azimuthal angle φ_{pr} of the Poynting vector with respect to the vertical direction as a function of the geomagnetic latitude. The value of $\varphi_{pr} = 0°$ corresponds to the southward direction of the wave vector, and the value of $\varphi_{pr} = 90°$ corresponds to its westward direction. Plots are based on the same events as in Figure 2.

The distribution of angles θ_{kr} and φ_{kr} with respect to the radial direction is color coded in Figures 2c and 2d, respectively, as a function of the geomagnetic latitude. *Z* axis in this case directs radially toward the center of the Earth, *x* axis directs to the geomagnetic south, and *y* axis is oriented westward. The θ_{kr} angle then represents the deviation of the wave vector from the downward vertical direction. The φ_{kr} angle shows the azimuth of the wave vector around the vertical direction. The wave vector points southward for $\varphi_{kr} = 0°$, and it points westward for $\varphi_{kr} = 90°$. The obtained results indicate the predominant downward propagation, with inclination toward the equator in midlatitudes.

The results obtained for the Poynting vector direction are shown in Figure 3a. According to the basic theory of electromagnetic waves in plasmas, the azimuthal angles of the Poynting vectors should be the same as the azimuthal angles of the wave vectors. We thus do not plot their distribution, and we only mention that this expectation is confirmed when we evaluate the Poynting vector directions experimentally. The distribution of the values of Poynting vector polar angles θ_{pB} shown in Figure 3a is again in agreement with the results obtained for the wave normal angles and the theory of electromagnetic waves in the cold plasma approximation.

The Poynting vectors are nearly parallel to $\mathbf{B_0}$ ($\theta_{pB} < 15°$) at higher latitudes in the Northern Hemisphere ($>55°$). The angle θ_{pB} is around 25° at latitudes from 15 to 50°, and it decreases to values $< 15°$ at the latitudes between 5 and 15° (i.e., again nearly parallel to $\mathbf{B_0}$). However, the Poynting vectors at the equatorial latitudes is oriented almost perpendicular to the geomagnetic field. The orientations of the Poynting vectors in the Southern Hemisphere are similar to those in the Northern Hemisphere, but they are antiparallel to the ambient magnetic field (i.e., the Poynting vectors are generally oriented away from the geomagnetic equator). There is a sudden change in the Poynting vector direction at the equator, and within about 5° from the geomagnetic equator the Poynting vectors seem to be mostly perpendicular to $\mathbf{B_0}$. This corresponds well to wave normal angles close to 90° observed in this latitudinal region in Figure 2a.

The deviation of the Poynting vector from the direction toward the Earth's center (θ_{pr} angle) is shown in Figure 3c as a function of the geomagnetic latitude. The φ_{pr} angle shown in Figure 3d corresponds to the azimuth of the Poynting vector around the vertical direction. The distribution of θ_{pr} angle shows oblique downward Poynting vectors at latitudes between −20° and +20°. Distribution of the φ_{pr} angle at these latitudes indicates that Poynting vectors are inclined outward from the equator. At higher latitudes we observe predominantly downward radial Poynting vectors for which the variation of the azimuthal angle is not relevant.

The distribution of the calculated values of ellipticity of the magnetic field fluctuations as a function of the geomagnetic latitude is color coded in Figure 3b. The obtained results are in agreement with the results obtained for the wave normal angles and the theory of electromagnetic waves in the cold plasma approximation. The waves are right-handed, nearly circular polarized ($E_B > 0.5$) in the whole range of the analyzed geomagnetic latitudes. The only exception is the region within about 5° from the geomagnetic equator, where the ellipticity seems to abruptly decrease to 0 again in agreement with the cold-plasma theory for R-X mode.

4. Discussion

While the wave vector directions observed at the DEMETER altitudes are nearly field-aligned at larger geomagnetic latitudes, they become gradually oblique at lower geomagnetic latitudes and, eventually, even perpendicular at the geomagnetic equator. They, however, always stay nearly perpendicular to the Earth's surface, directed downward to the Earth. This high latitude region corresponds to L shells > 3 which is likely a region close to the magnetic field tube where these emissions could be generated [*Titova et al*., 2015]. The observed nearly field-aligned wave vectors might be consistent with ducted propagation of QP emissions from the source region down to the low altitude at higher latitudes, in agreement with the results observed by *Manninen et al*. [2014]. Similar effect can be, however, also consistent with unducted propagation from a source generating waves at high wave normal angles [*Santolík et al*., 2006b]. The propagation pattern of QP emissions observed at higher geomagnetic latitudes is also similar to previous observations by the Freja spacecraft [*Santolík and Parrot*, 1999] and to simulation results of the whistler mode wave propagation by *Bortnik et al.* [2011]. Such waves can propagate from their origin to the higher latitudes where they enter into the plasmasphere, then moving earthward to lower altitudes where they were observed by DEMETER. This is also consistent with statistical properties of intense whistler mode waves which appear to be mostly field aligned [*Santolík et al*., 2014] during the propagation from their source region.

There are two particular features in the latitudinal dependence of the wave propagation parameters, which deserve further attention. First, there is a change in behavior of the wave parameters at the latitudes of about ±50°. This change is might be related to the plasmapause effects. The projection of an average plasmapause position to DEMETER altitudes is at latitudes about ±60° [*McPherson and Koons*, 1970]. Whistler mode waves guided by the plasmapause can deflect at altitudes of a few thousand of kilometers, and they can propagate at lower latitudes [*Inan and Bell,* 1977], hence possibly explaining the change at ±50°.

The second important feature is the behavior of the wave parameters close to the geomagnetic equator. Although the amount of data at low latitudes is limited, it appears that the perpendicular propagation of the waves close to the equator is a real effect. We note that such propagation is possible only for frequencies lower than the lower hybrid frequency. This would suggest a presence of an additional group of QP emissions which propagate from larger radial distances close to the equatorial plane. It might correspond to low-altitudinal observations of recently reported equatorial noise with a quasiperiodic modulation [*Boardsen et al*., 2014; *Fu et al*., 2014; *Němec et al*., 2015]. This type of QP emissions is generated with wave vectors nearly perpendicular to the geomagnetic field by instable ion distributions [*Gurnett*, 1976] at frequencies below the lower hybrid frequency. Taking into account that the frequencies of the observed waves are generally larger than about 500 Hz, this would indicate that the source region of these emissions has to be at radial distances lower than about 3.4 R_E.

In summary, the observed QP emissions exhibit a propagation pattern with a changing wave normal direction with respect to the local geomagnetic field. This probably reflects different regions through which the waves propagate and possibly also their different source mechanisms. The observed wave vectors are, however, always nearly perpendicular to the Earth's surface, allowing the waves to propagate through ionosphere and

to be subsequently detected on the ground. Our results thus can contribute to explanation of QP occurrence in the ground-based VLF recordings [*Manninen et al.*, 2013, 2014; *Titova et al.*, 2015].

Acknowledgments
This investigation is based on observations performed by the DEMETER satellite launched by the Centre National d'Etudes Spatiales. The authors thank J.J. Berthelier, the PI of the ICE instrument, for the use of the data. This work was supported by the P209/11/2280, 14-31899S, and 15-01775Y grants of the Grant Agency of the Czech Republic, by the LH15304 grant, and by the Praemium Academiae award; the work of M.P. is supported by the Centre National d'Etudes Spatiales.

References

Berthelier, J. J., et al. (2006), ICE, the electric field experiment on DEMETER, *Planet. Space Sci.*, *54*, 456–471.
Bespalov, P. A., and V. Y. Trakhtengerts (1976), The dynamics of the cyclotron instability in a magnetic trap, *Fiz. Plazmy*, *2*(3), 397–406.
Boardsen, S. A., G. B. Hospodarsky, C. A. Kletzing, R. F. Pfaff, W. S. Kurth, J. R. Wygant, and E. A. MacDonald (2014), Van Allen Probe observations of periodic rising frequencies of the fast magnetosonic mode, *Geophys. Res. Lett.*, *41*, 8161–8168, doi:10.1002/2014GL062020.
Bortnik, J., L. Chen, W. Li, R. M. Thorne, and R. B. Horne (2011), Modeling the evolution of chorus waves into plasmaspheric hiss, *J. Geophys. Res.*, *116*, A08221, doi:10.1029/2011JA016499.
Carson, W. B., J. A. Koch, J. H. Pope, and R. M. Gallet (1965), Long-period very low frequency emission pulsations, *J. Geophys. Res.*, *70*, 4293–4303.
Davidson, G. T. (1979), Self-modulated VLF wave-electron interactions in the magnetosphere: A cause of auroral pulsations, *J. Geophys. Res.*, *84*, 6517–6523.
Demekhov, A. G., and V. Y. Trakhtengerts (1994), A mechanism of formation of pulsating aurorae, *J. Geophys. Res.*, *99*, 5831–5841.
Engebretson, M. J., J. L. Posch, A. J. Halford, G. A. Shelburne, A. J. Smith, M. Spasojević, U. S. Inan, and R. L. Arnoldy (2004), Latitudinal and seasonal variations of quasi-periodic and periodic VLF emissions in the outer magnetosphere, *J. Geophys. Res.*, *109*, A05216, doi:10.1029/2003JA010335.
Fu, H. S., J. B. Cao, Z. Zhima, Y. V. Khotyaintsev, V. Angelopoulos, O. Santolík, Y. Omura, U. Taubenschuss, L. Chen, and S. Y. Huang (2014), First observation of rising-tone magnetosonic waves, *Geophys. Res. Lett.*, *41*, 7419–7426, doi:10.1002/2014GL061867.
Gurnett, D. A. (1976), Plasma wave interactions with energetic ions near the magnetic equator, *J. Geophys. Res.*, *81*, 2765–2770.
Hayosh, M., D. L. Pasmanik, A. G. Demekhov, O. Santolík, M. Parrot, and E. E. Titova (2013), Simultaneous observations of quasi-periodic ELF/VLF wave emissions and electron precipitation by DEMETER satellite: A case study, *J. Geophys. Res. Space Physics*, *118*, 4523–4533, doi:10.1002/jgra.50179.
Hayosh, M., F. Němec, O. Santolík, and M. Parrot (2014), Statistical investigation of VLF quasi-periodic emissions measured by the DEMETER spacecraft, *J. Geophys. Res. Space Physics*, *119*, 8063–8072, doi:10.1002/2013JA019731.
Helliwell, R. A. (1965), *Whistlers and Related Ionospheric Phenomena*, Stanford Univ. Press, Stanford, Calif.
Ho, D. (1973), Interaction between whistlers and quasi-periodic VLF emissions, *J. Geophys. Res.*, *78*, 7347–7356.
Inan, U. S., and T. F. Bell (1977), The plasmapause as a VLF wave guide, *J. Geophys. Res.*, *82*(19), 2819–2827, doi:10.1029/JA082i019p02819.
Kimura, I. (1974), Interrelation between VLF and ULF emissions, *Space Sci. Rev.*, *16*, 389–411.
Kitamura, T., J. A. Jacobs, T. Watanabe, and J. R. B. Flint (1968), Investigation of quasi-periodic VLF emissions and their relation to geomagnetic micropulsations, *Nature*, *220*, 360–361.
Kitamura, T., J. A. Jacobs, and T. Watanabe (1969), An investigation of quasi-periodic VLF emissions, *J. Geophys. Res.*, *74*, 5652–5664.
Manninen, J., N. G. Kleimenova, O. V. Kozyreva, P. A. Bespalov, and T. Raita (2012), Quasi-periodic very low frequency emissions, very low frequency chorus, and geomagnetic *Pc*4 pulsations (Event on April 3, 2011), *Geomagn. Aeron.*, *52*(1), 77–87.
Manninen, J., N. G. Kleimenova, O. V. Kozyreva, P. A. Bespalov, and A. E. Kozlovsky (2013), Non-typical ground-based quasi-periodic VLF emissions observed at L ~ 5.3 under quiet geomagnetic conditions at night, *J. Atmos. Sol. Terr. Phys.*, *99*, 123–128, doi:10.1016/j.jastp.2012.05.007.
Manninen, J., A. G. Demekhov, E. E. Titova, A. E. Kozlovsky, and D. L. Pasmanik (2014), Quasiperiodic VLF emissions with short-period modulation and their relationship to whistlers: A case study, *J. Geophys. Res. Space Physics*, *119*, 3544–3557, doi:10.1002/2013JA019743.
McPherson, D. A., and H. C. Koons (1970), Dependence of ELF emissions on the location of the plasmapause, *J. Geophys. Res.*, *75*, 5559–5564, doi:10.1029/JA075i028p05559.
Morrison, K., M. J. Engebretson, J. R. Beck, J. E. Johnson, R. L. Arnoldy, J. L. J. Cahill, D. L. Carpenter, and M. Gallani (1994), A study of quasi-periodic ELF-VLF emissions at three antarctic stations: Evidence for off-equatorial generation?, *Ann. Geophys.*, *12*, 139–146, doi:10.1007/s0058599401398.
Němec, F., O. Santolík, M. Parrot, J. S. Pickett, M. Hayosh, and N. Cornilleau-Wehrlin (2013a), Conjugate observations of quasi-periodic emissions by Cluster and DEMETER spacecraft, *J. Geophys. Res. Space Physics*, *118*, 198–208, doi:10.1029/2012JA018380.
Němec, F., O. Santolík, J. S. Pickett, M. Parrot, and N. Cornilleau-Wehrlin (2013b), Quasi-periodic emissions observed by the Cluster spacecraft and their association with ULF magnetic pulsations, *J. Geophys. Res. Space Physics*, *118*, 4210–4220, doi:10.1002/jgra.50406.
Němec, F., O. Santolík, Z. Hrbackova, J. S. Pickett, and N. Cornilleau-Wehrlin (2015), Equatorial noise emissions with quasiperiodic modulation of wave intensity, *J. Geophys. Res. Space Physics*, *120*, 2649–2661, doi:10.1002/2014JA020816.
Parrot, M., et al. (2006), The magnetic field experiment IMSC and its data processing onboard DEMETER: Scientific objectives, description and first results, *Planet. Space Sci.*, *54*, 441–455.
Pasmanik, D. L., E. E. Titova, A. G. Demekhov, V. Y. Trakhtengerts, O. Santolík, F. Jiricek, K. Kudela, and M. Parrot (2004), Quasi-periodic ELF/VLF wave emissions in the Earth's magnetosphere: Comparison of satellite observations and modeling, *Ann. Geophys.*, *22*, 4351–4361.
Santolík, O., and M. Parrot (1999), Case studies on wave propagation and polarization of ELF emissions observed by Freja around the local proton gyro-frequency, *J. Geophys. Res.*, *104*, 2459–2475.
Santolík, O., F. Lefeuvre, M. Parrot, and J. L. Rauch (2001), Complete wave-vector directions of electromagnetic emissions: Application to INTERBALL-2 measurements in the nightside auroral zone, *J. Geophys. Res.*, *106*, 13,191–13,201.
Santolík, O., J. S. Pickett, D. A. Gurnett, and L. R. O. Storey (2002), Magnetic component of narrowband ion cyclotron waves in the auroral zone, *J. Geophys. Res.*, *107*(A12), 1444, doi:10.1029/2001JA000146.
Santolík, O., M. Parrot, and F. Lefeuvre (2003), Singular value decomposition methods for wave propagation analysis, *Radio Sci.*, *38*(1), 1010, doi:10.1029/2000RS002523.
Santolík, O., F. Němec, M. Parrot, D. Lagoutte, L. Madrias, and J. J. Berthelier (2006a), Analysis methods for multi-component wave measurements on board the DEMETER spacecraft, *Planet. Space Sci.*, *54*, 512–527.
Santolík, O., J. Chum, M. Parrot, D. A. Gurnett, J. S. Pickett, and N. Cornilleau-Wehrlin (2006b), Propagation of whistler mode chorus to low altitudes: Spacecraft observations of structured ELF hiss, *J. Geophys. Res.*, *111*, A10208, doi:10.1029/2005JA011462.
Santolík, O., E. Macúšová, I. Kolmašová, N. Cornilleau-Wehrlin, and Y. de Conchy (2014), Propagation of lower-band whistler-mode waves in the outer Van Allen belt: Systematic analysis of 11 years of multi-component data from the Cluster spacecraft, *Geophys. Res. Lett.*, *41*, 2729–2737, doi:10.1002/2014GL059815.
Sato, N., and H. Fukunishi (1981), Interaction between ELF-VLF emissions and magnetic pulsations: Classification of quasi-periodic ELF-VLF emissions based on frequency-time spectra, *J. Geophys. Res.*, *86*, 19–29.

Sato, N., and S. Kokubun (1980), Interaction between ELF-VLF emissions and magnetic pulsations: Quasi-periodic ELF VLF emissions associated with Pc 3-4 magnetic pulsations and their geomagnetic conjugacy, *J. Geophys. Res.*, *85*, 101–113.

Sato, N., K. Hayashi, S. Kokubun, T. Oguti, and H. Fukunishi (1974), Relationships between quasi-periodic VLF emission and geomagnetic pulsation, *J. Atmos. Terr. Phys.*, *36*, 1515–1526.

Sazhin, S. S. (1987), An analytical model of quasi-periodic ELF-VLF emissions, *Planet. Space Sci.*, *35*(10), 1267–1274.

Titova, E. E., B. V. Kozelov, A. G. Demekhov, J. Manninen, O. Santolík, C. A. Kletzing, and G. Reeves (2015), Identification of the source of quasiperiodic VLF emissions using ground-based and Van Allen Probes satellite observations, *Geophys. Res. Lett.*, *42*, 6137–6145, doi:10.1002/2015GL064911.

Tixier, M., and N. Cornilleau-Wehrlin (1986), How are the VLF quasi-periodic emissions controlled by harmonics of field line oscillations? The results of a comparison between ground and GEOS satellites measurements, *J. Geophys. Res.*, *91*, 6899–6919.